Research Article / Review Article FUPRE JOURNAL 6(4): 118-136(2022)

FUPRE Journal of Scientific and Industrial Research

ISSN: 2579-1184(Print) ISSN: 2578-1129 (Online)

https://fupre.edu.ng/journal

Electronic, thermodynamic, and effect of pressure on mechanical properties in CoTiSb and CoTiBi semi-Heuslers

Nenuwe, O. N.[1,*], Omagbemi, O.[2]

[1] *Department of Physics, Federal University of Petroleum Resources, Effurun, Delta State, Nigeria*

ARTICLE INFO

Received: 20/09/2022

Accepted: 25/10/2022

Keywords

CoTiBi, semi-Heusler, mechanical properties, phonon dispersion, heat capacity.

ABSTRACT

First principles technique based on density functional theory (DFT) is employed to study the structural, phonon, electronic, thermodynamic, and mechanical properties of CoTiSb and CoTiBi semi-Heuslers. The optimized structural parameters including lattice constant, bulk modulus, and formation energy were determined in three structural phase. The results obtained were found to be in agreement with available experimental and other theoretical results. CoTiSb and CoTiBi were found to be brittle, mechanically, dynamically, and thermodynamically stable, and exhibit an indirect band gap semiconductor property as revealed by the bandstructure, total and projected density of states. The effect of pressure on the elastic, and mechanical behaviors were investigated in a range of 0 – 30 GPa. Thermodynamic properties of CoTiSb and CoTiBi were calculated from 0 – 800 K. At room temperature, the Debye heat capacity (C_v) was found to be 68.6 and 70.43 *J/K/mol* for CoTiSb and CoTiBi. At low temperature, C_v, obeys the Debye power-law ($C_v \propto T^3$), and at eleviated temperature, C_v, agrees with the Dulong-Pitit law, and converged at a value of 73.94 and 74.22 *J/K/mol* for CoTiSb and CoTiBi, respectively. For the first time results have been obtained for CoTiBi semi-Heusler. These results may serve as reference to further studies.

1. INTRODUCTION

Full Heusler (FH) and semi-Heusler (SH) compounds have attracted worldwide interest due to their promising applications in optoelectronics, spintronics, and thermoelectrics (Benzoudji et al., 2019; Casper et al., 2012; Chadov et al., 2010; Hermet et al., 2013; Kieven et al., 2010; Fang et al., 2017). They possess high Currie temperature, semiconducting and semi-metallic properties. The full Heuslers have a general formula X_2YZ, while XYZ represents semi-Heusler systems. The Z-atom belongs to the sp-block of the periodic-table, while Y and X are transition-metals. The SHs possess a $C1_b$ structure with space group F-43m. The X, Y, Z atoms occupy the 4a (0, 0, 0), 4b (0.5, 0.5, 0.5), and 4c (0.25, 0.25, 0.25), with 4d (0.75, 0.75, 0.75) left vacant, while the FH occupies all four sites in the Wyckoff coordinates.

Recently, many SH alloys have been studied (Dey et al., 2021; Dutt et al., 2022; Enamullah et al., 2020; Osafile & Nenuwe, 2021; Parvin et al., 2021; Rogl et al., 2016; Sarwan et al., 2021). Semi-Heuslers are found to be thermally and mechanically stable and possess substantial thermoelectric power factor jaishi (Ahmad Khandy et al., 2021; Jaishi et al., 2021; Javed et al., 2020; Kieven et al., 2010; Rogl et al., 2016). These attributes qualify semi-Heusler materials for high-temperature

Corresponding author: nenuwe.nelson@fupre.edu.ng

DIO

thermoelectric (TE) applications.

Amazingly, many extrinsic semiconductors exhibit good TE behavior with values of figure of merit (*zT*) comparable to the well-known silicon, lead, and bismuth-based TE compounds like SiGe, PbTe, BiSb BiSbTe, and Bi_2Te_3 (Goldsmid & Douglas, 1954; Jaishi et al., 2021; Lee et al., 2012; Poudel et al., 2008; Poudeu et al., 2006). However, larger data of lattice thermal conductivity reduce the *zT* for intrinsic SH alloys. Studies have confirmed that the decline of thermal conductivity by doping of ZrCoBi (Zhu et al., 2018), TaFeSb (Zhu et al., 2019), and FeNbSb (Fu et al., 2015) SH alloys resulted in a significant improvement of the *zT*. Pressure application has also improved TE properties of SHs (Jaishi et al., 2021; Kumarasinghe & Neophytou, 2019).

Therefore, it is clear that SHs are good materials for TE applications, but some will require expensive dopants to diminish the lattice thermal conductivity and adjust the carrier concentration. Hence, further studies are needed to find efficient, non-harmful, economical, and abundant multifunctional materials (Jaishi et al., 2021). Also, SHs have attracted attention due to the possible adjustable band gap (Kumarasinghe & Neophytou, 2019), high optical absorption, and optical conductivity in the band range of the incident spectrum (Kieven et al., 2010; Wei & Wang, 2018). The noticeable band gap becomes useful in optoelectronic applications, and they act as a potential source to replace Pb-containing compounds (Eperon et al., 2015; Ramasamy et al., 2016). From our literature review, we noticed very few theoretical studies on Co-based SH, and in particular, no published data was found for CoTiBi.

Consequently, in this study, we utilised DFT to carry out a thorough examination of the structural, electronic, and phonon characteristics as well as the impact of pressure on the mechanical, thermodynamic, and elastic properties of CoTiSb and CoTiBi semi-Heuslers.

2. MATERIALS AND METHODS

The elastic, mechanical, thermodynamic, structural, and electronic properties of CoTiSb and CoTiBi semi-Heuslers were studied based on the density functional technique (Schwarz et al., 2002; Schwarz & Blaha, 2003; Sjöstedt et al., 2000). The full potential augmented plane waves plus local orbitals (FP-LAPW+lo) was used to approximate the Kohn-Sham equation, and the generalized-gradient-approximation was employed to solve the exchange correlation potential (Perdew et al., 1997). The elastic, mechanical, thermodynamic, and electronic properties were obtained from the WIEN2K computational package (Jamal et al., 2014), and the phonon dispersion properties were extracted from the Thermo-pw code implemented in Quantum Expresso (Malica & Dal Corso, 2021). In the WIEN2K, the input data such as *l*max, *k*-points, and *RK*max were chosen to be 10, 5,000, and 8.5, respectively. The *k*-points and *E*cut in the Thermo_pw package were optimized to (4 x 4 x 4**)** and 80, respectively.

3. RESULTS AND DISCUSSION

3.1 Structural and dynamical stability and electronic properties

The CoTiBi and CoTiSb semi-Heuslers crystalize in the cubic crystal structure in space group F-43m (No. 216) as a non-magnetic semiconductor. From the well-known Wyckoff atomic positions for the semi-Heusler alloys XYZ (4a(0, 0, 0), 4b(0.5, 0.5, 0.5), 4c(0.25, 0.25, 0.25)), three structural types are derived. We studied CoTiBi and CoTiSb alloys in three phases: α=(4c, 4b, 4a), β= (4b, 4a, 4c), and γ=(4a, 4c, 4b) . The lattice constants and bulk modulus have been obtained by calculating the total energy for several volumes and fitted into the Murnaghan equation of states (Murnaghan, 1944; Tyuterev & Vast, 2006).

$$E - E_0 = \left[\frac{E_0}{B'} + \frac{V_0}{B'(B'-1)} + \frac{1}{(1-B')}\right] \quad (1)$$

B and B' represent bulk modulus and pressure derivative of B. E_0 is the ground state energy, and V_0 is the equilibrium volume. To determine the minimum energy for the α-, β-, and γ-phases, as shown in Figure 1, we used Eq. (1) to plot the total energy against variation in volume. For both semi-Heuslers, the α-phase was discovered to have the lowest ground state energy, indicating that it is the most stable structural phase for both SHs. Table 1 reports the structural properties for the CoTiBi and CoTiSb SHs, and our findings are in conformity with the available data (Ma et al., 2017; Ouardi et al., 2012; Shi et al., 2017; Toboła et al., 1998).

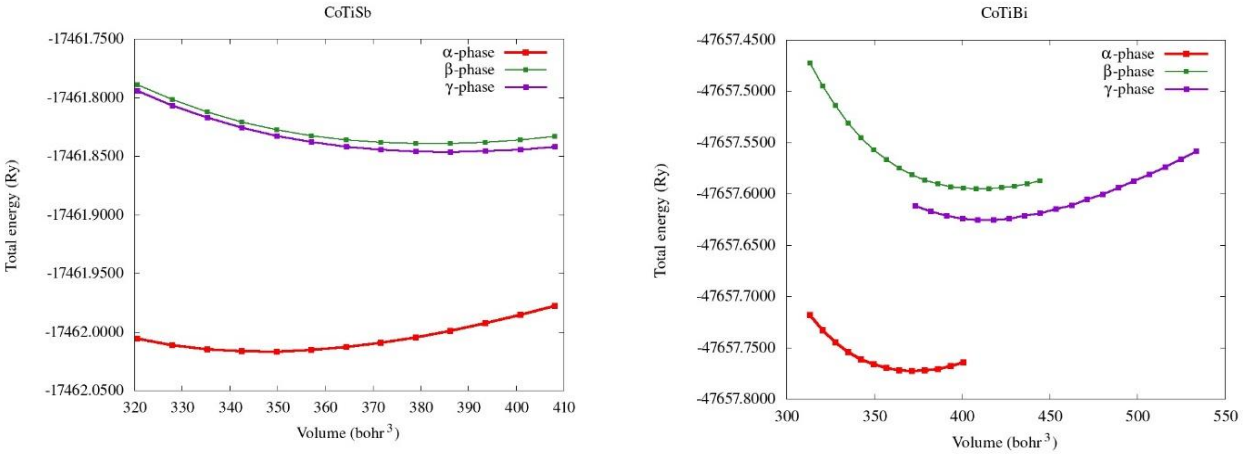

Figure 1: Calculated total energy versus volume for (Type 1, Type 2, Type 3) structural phases of CoTiSb and CoTiBi semi-Heuslers.

Table 1: Calculated data of lattice parameters a_0 (Å), bulk modulus B (GPa), band gap E_g (eV), minimum energy E_m (Ry), and formation energy (E_f).

Semi-Heuslers	**Phase**	**a_0**	**E_m**	**E_f**	**B**	**E_g**
	α	6.04	-47,657.772783	-0.048	122.06	0.91
CoTiBi	β	6.25	-47,657.625283	0.0012	90.00	-
	γ	6.24	-47,657.595424	0.0111	95.76	-
CoTiSb	α	5.90	-17,462.016904	-0.069	142.63	1.05
		5.88		-0.67	142	1.06
		5.88				0.95
		5.90				1.03
	β	6.09	-17,461.839494	-0.01	110.42	-
	γ	6.11	-17,461.846274	-0.012	102.75	-

***References**: (Ouardi et al., 2012; Ma et al., 2017; Toboła et al., 1998; Shi et al., 2017).*

Also, the formation energy was computed using the relation in Eq.(2) (Z. W. Huang et al., 2012; Yakoubi et al., 2012) to establish the structural stability and feasibility of the studied SH compounds.

$$E_f = \frac{E_T - xE_{C_0} - yE_{T_i} - zE_{B_i(Sb)}}{(x+y+z)} \quad (2)$$

where E_{Co}, E_{Ti}, E_{Bi}, and E_{Sb} are the total energies of the pure elements *Co, Ti, Bi*, and *Sb*, respectively; E_T is the total energy of the SH alloy; and *x, y*, and *z* are the numbers of *Co, Ti, Bi*, and *Sb* atoms in the primitive cell, respectively. Table 1 displays the values of minimal energy, energy of individual elements, and resultant formation energy. We discovered that the α-phase formation energy is negative, indicating that the formation and feasibilty of CoTiBi and CoTiSb are possible.

Figure 2 depicts the phonon dispersion and phonon density of states for CoTiBi and CoTiSb. There are six optical and three acoustic modes in these semi-Heuslers since each unit cell has three atoms. The fact that all vibration modes in Figure 2 are positive confirmed the dynamical stability of these compounds. For CoTiSb and CoTiBi, respectively, the highest optical branches have frequencies of 312.51 cm^{-1} and 264.04 cm^{-1}. We noticed that, due to an increase in atomic mass, the frequency of CoTiSb to CoTiBi decreased (Guo et al., 2015). The non-appearance of imaginary frequencies in the phonon scattering curve shows that CoTiBi and CoTiSb are thermodynamically stable materials.

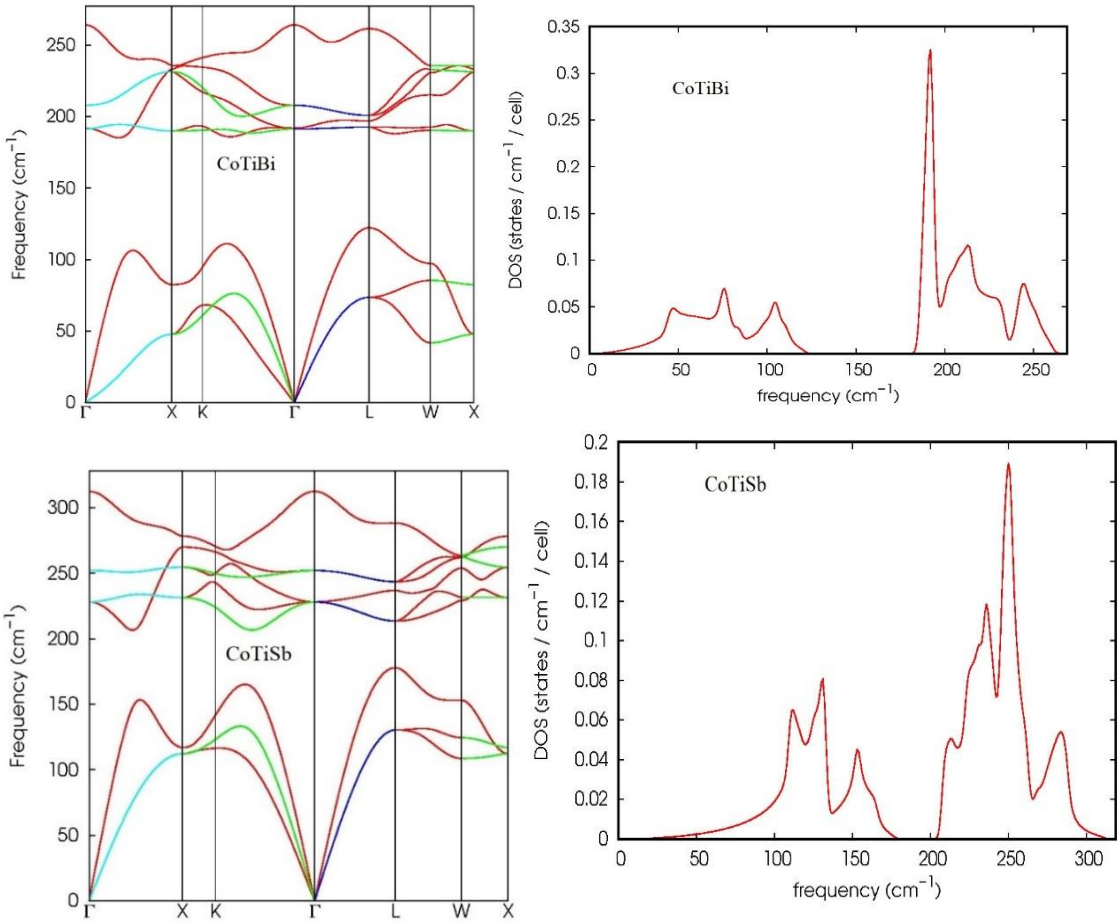

Figure 2: Phonon dispersion and phonon density of states for CoTiBi and CoTiSb.

The considered electronic bandstructures along the high symmetry *k*-points are

presented in Figure 3**.** According to (Kaur & Kumar, 2017), the presence of an electronic band in semi-Heuslers with 18-valence electrons is mainly due to *d*-orbitals. In Figure 3, the conduction band (CB) minimum is located at *X* high symmetry point, and the valence band (VB) maximum is located at Γ point, which implies that both CoTiBi and CoTiSb are indirect band gap semiconductors with an energy gap of 0.91 and 1.05 eV, respectively. The calculated band gap for CoTiSb is (1%) less than that reported in Ref. (Ouardi et al., 2012), in line with the fact that the band gap obtained from GGA underestimates experimental values. Also, our result is 9.5% and 1.9% higher than the results obtained using the Korringa-Kohn-Rostoker method (Toboła et al., 1998) and Heyd-Scuseria-Ernzerhof (HSE06) hybrid functional (Shi et al., 2017), as shown in Table 1. However, the literature has no data on band gap and lattice parameters to compare results obtained for CoTiBi alloy. Therefore, results obtained for CoTiBi semi-Heusler can be used as a reference for further studies.

The projected density of states (PDOS) and total density of states (TDOS) for CoTiSb and CoTiBi, respectively, are calculated and shown in Figures 4 and 5, respectively, to analyse the contributions of various atomic orbitals to the band gap. Figures (4a and 5a) show that for both semi-Heuslers, the *d, d-eg, d-t2g* orbitals of the *Y* and *X* atoms (Ti and Co) make majority contributions to the energy gap from both VB and CB. The TDOS: Figures (4b and 5b) show that both the up-spin and down-spin channels in the spin-polarized state of these materials have an energy gap, proving that CoTiSb and CoTiBi are pure semiconductors in both channels. Additionally, we noticed that the Fermi level (E_f), which is known to move towards the CB for n-type and VB for p-type extrinsic semiconductors, shifts towards the valence bands in Figures (3, 4 & 5), indicating that CoTiSb and CoTiBi semi-Heuslers are likely to function better as p-type semiconductors (Jhi et al., 1999).

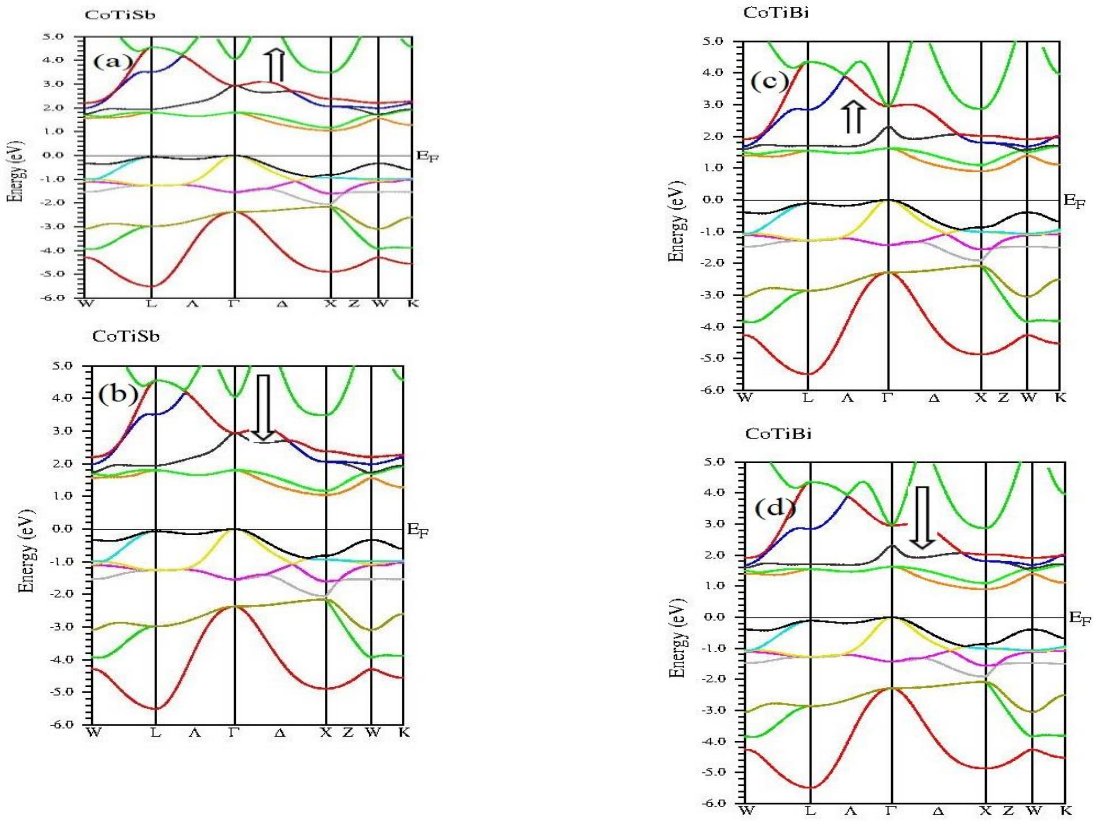

Figure 3: Bandstructure of up spin (a, c) and down spin (b, d) for CoTiSb and CoTiBi

semi-Heuslers.

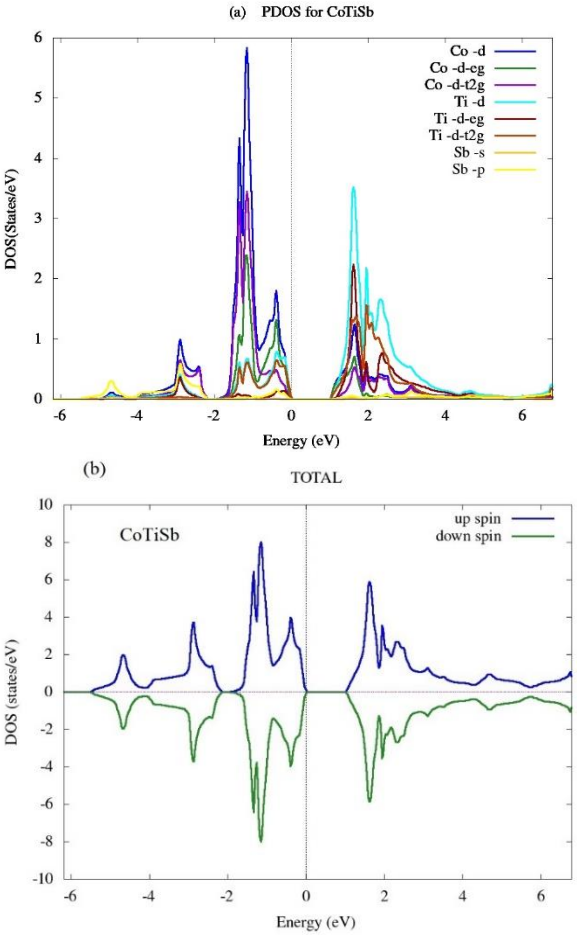

Figure 4: (a) Projected density of states, and (b) Total density of states for CoTiSb semi-Heusler.

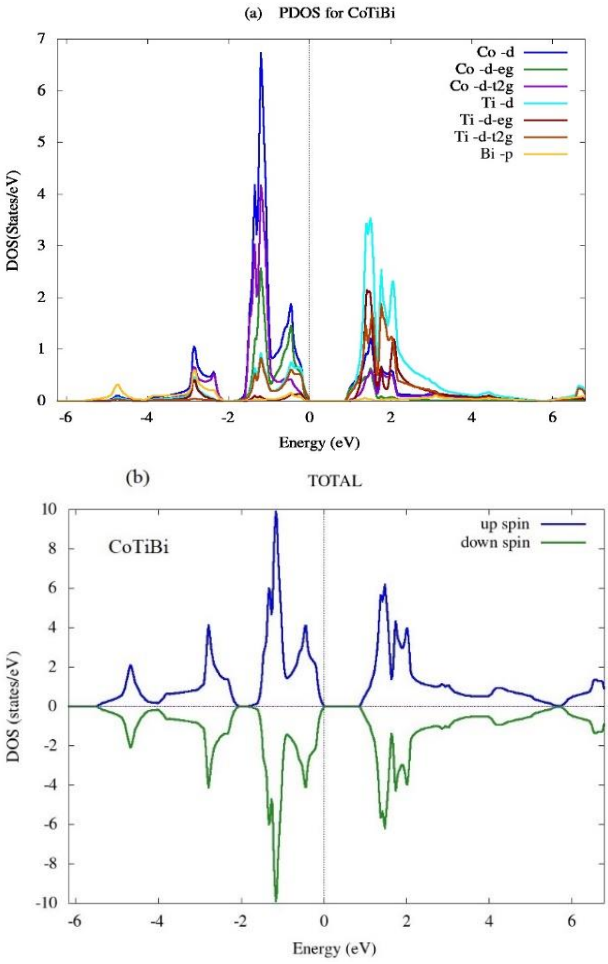

Figure 5: (a) Projected density of states, and (b) Total density of states for CoTiBi semi-Heusler.

3.2 Elastic constants

Elastic constants are crucial properties of solid state materials. They are employed to ascertain how a crystal reacts to external forces and provides crucial information about the types of forces operating in a crystal structure (Mehl, 1993). Also, elastic constants can provide important data such as Young, bulk, and shear moduli, Poisson ratio, Pugh ratio, isotropic factor, stiffness, ductility, stability, and brittleness of materials. In order to stay within the elastic domain of the crystal structure, only small lattice distortions were used, leading to the determination of the second-order elastic constants (C_{ij}) for cubic CoTiBi and CoTiSb compounds at 0 K and zero pressure (Wang et al., 1993). A cubic crystal structure is known to have three different elastic constants (C_{11}, C_{12}, C_{44}). Table 2 contains the elastic constants of CoTiBi and CoTiSb that were calcuated for this study. According to the Born stability conditions, the cubic elastic constants must satisfy the following requirements (Wang et al., 1993) in Eq. (3). All calculated elastic constants of CoTiBi and CoTiSb semi-Heuslers satisfy Eq. (3), indicating that these semi-Heusler alloys are mechanically stable. The results in Table 2 agree with the values reported by Siham Ouardi et al. (Ouardi et al., 2012),

where they studied the transport and mechanical behaviors of pure and doped CoTiSb compounds.

$$C_{11} - C_{12} > 0, \quad C_{44} > 0, \text{ and } C_{11} + 2C_{12} > 0 \tag{3}$$

Table 2: Calculated values of the elastic constants (C_{ij}), Young's modulus (E), bulk modulus (B), and shear modulus (G) in GPa, Poisson ratio (v), isotropic factor (A), Pugh ratio, Cauchy pressure and melting temperature (T_m) for CoTiBi and CoTiSb semi-Heuslers.

Compound	C_{11}	C_{12}	C_{44}	B	G	E	V	A	B/G	C_{12} - C_{44}	T_m (K) ±300
CoTiBi	221.93	73.34	75.11	122.88	74.78	186.51	0.25	1.01	1.64	-1.77	1864.63
CoTiSb	258.50	75.22	95.88	136.31	94.16	229.61	0.22	1.05	1.45	-20.66	2028.74
	259	84	93	142	91	224	0.24	1.06	1.56	-9	-

***Reference**: (Ouardi et al., 2012).*

It is well established that pressure has a considerable impact on the elastic and mechanical properties of materials (Hill, 1952; Jiao et al., 2013; Korozlu et al., 2013; Nelson and Judith, 2021; Nenuwe and Agbalagba, 2021; Sailuam et al., 2022) (Wani et al., 2021). In this study, we investigated how pressure affects the mechanical and elastic characteristics of CoTiBi and CoTiSb SHs. At applied hydrostatic pressure in the range of (5 - 30) GPa, we presented the elastic constants of CoTiBi and CoTiSb semi-Heuslers in Table 3 in steps of 5 GPa. To the best of our knowledge, the elastic constants of CoTiBi and CoTiSb under pressure have not been published in the literature. Also, we plot the pressure-dependent behavior of elastic constants of CoTiBi and CoTiSb SH as shown in Figure 6. We observed that pressure significantly enhanced the elastic constants C_{ij}, and the values of C_{11} are higher than C_{12}, and C_{44} within the entire range of pressure considered. The C_{12}, and C_{44} are shear elastic constants and signify elasticity in shape. While C_{11} signifies elasticity in length. The calculated C_{11} and C_{44} for CoTiSb are higher than those of CoTiBi, which suggests that the strength of CoTiSb is higher than CoTiBi alloy. The Cauchy pressure (C_{12} - C_{44}) provides information about bonding in a cubic material. A negative Cauchy pressure ($C_{44} > C_{12}$) signifies a covalently bonded solid, while positive Cauchy pressure ($C_{44} < C_{12}$) represents ionic bonding. Also, Cauchy pressure predicts that positive values indicate ductility while negative values indicate brittleness for a given material. The data at zero pressure in Table 2 shows that these compounds are covalently bonded and are brittle. This agree with the negative value reported in REF. (Ouardi et al., 2012) for CoTiSb. In Table 3, the Cauchy pressure is negative as pressure rises from 5 – 15 GPa and 25 – 30 GPa. At the pressure value of 20 GPa, the Cauchy pressure was positive, implying that CoTiBi compound is brittle when pressure rises from 0 – 15 GPa, and 25 – 30 GPa. Moreover, at 20 GPa, CoTiBi behaves like a ductile material, which may be associated with a phase transition that might have occurred around 20 GPa pressure

Table 3: Calculated values of the elastic constants C_{ij} (GPa) and Cauchy pressure under different pressure for CoTiBi and CoTiSb semi-Heuslers

Materials	Pressure	C_{11}	C_{12}	C_{44}	C_{12} - C_{44}
	5	258.81	88.00	88.55	-0.55
	10	298.90	98.66	105.07	-6.41
CoTiBi	15	332.86	110.92	118.95	-8.03
	20	372.79	133.75	130.96	2.79
	25	408.62	144.14	145.33	-1.19
	30	437.85	151.78	159.68	-7.9
	5	297.51	96.84	107.17	-10.33
	10	332.98	105.04	116.88	-11.84
CoTiSb	15	366.04	115.60	127.01	-11.41
	20	396.29	124.32	139.82	-15.5
	25	431.0	134.39	154.78	-20.39
	30	456.88	141.19	166.75	-25.56

3.3 Mechanical properties

The bulk modulus (B), Young modulus (E), shear modulus (G), Poisson ratio (v), isotropy factor (A), and Pugh ratio are important mechanical behaviors of materials that can be calculated from the elastic constants of solid materials using the Voigt-Reuss-Hill average technique (Huang et al., 2014).

$$B = \frac{1}{3}(C_{11} + 2C_{12}) \quad (4)$$

$$B_V = B_R = B \quad (5)$$

$$G = \frac{1}{2}(G_v + G_R) \quad (6)$$

$$G_R = \frac{5(C_{11}-C_{12})C_{44}}{3(C_{11}-C_{12})+4C_{44}} \quad (7)$$

$$G_v = \frac{1}{5}(C_{11} - C_{12} + 3C_{44}) \quad (8)$$

$$E = \frac{9BG}{3B+G} \quad (9)$$

$$A = \frac{2C_{44}}{C_{11}-C_{12}} \quad (10)$$

$$v = \frac{3B-2G}{2(3B+G)} \quad (11)$$

The Reuss and Voigt approximations of G and B are respectively, G_R, G_v, B_R, and B_v. Table 4 provides a list of the computed mechanical properties. Shear modulus (G) demonstrates how resistant a material is to plastic deformations under shear stress, while the bulk modulus (B) measures a material's resistance to volume changes brought on by applied pressure (Ali & Rahaman, 2018; Boucetta, 2014). Figure 7 shows how pressure affects E, G, and B. As can be observed, all the parameters respond virtually linearly to changes in external pressure. According to Figure 7, the values of the bulk modulus B and shear modulus G for CoTiBi and CoTiSb, respectively, at a pressure of 5 GPa are 144.94 and 87.27 GPa and 163.73 and 104.38 GPa, respectively. B

and *G* have 247.14 and 152.79 GPa for CoTiBi and 246.42 and 163.13 GPa for CoTiSb when the pressure hits 30 GPa**.** The findings of the current calculations show that the bulk modulus is more pressure sensitive than the shear modulus. A significant quantity is the Young's modulus *E*, which is the proportion of tensile stress to tensile strain (Pugh, 1954). It serves as a gauge for determining solid rigidity. The higher the value of *E*, the more rigid the material is. Table 4 shows that the computed value of *E* grows practically linearly with pressure, demonstrating that the pressure significantly affects the stiffness of CoTiBi and CoTiSb compounds.

Table 4: Calculated values of Young's modulus (*E*), bulk modulus (*B*),v and shear modulus (*G*) in GPa, Poisson ratio (*v*), isotropic factor (*A*), and Pugh ratio under different pressure for CoTiBi and CoTiSb semi-Heuslers

Materials	**Pressure**	***B***	***G***	***E***	***B/G***	***V***	***A***
	5	144.94	87.27	218.06	1.66	0.25	1.03
	10	165.41	103.06	256.01	1.60	0.24	1.05
CoTiBi	15	184.90	115.69	287.17	1.60	0.24	1.07
	20	213.43	126.25	316.38	1.69	0.25	1.10
	25	232.30	140.94	349.62	1.64	0.25	1.10
	30	247.14	152.79	380.07	1.62	0.24	1.12
	5	163.73	104.38	258.26	1.57	0.24	1.07
	10	181.02	115.71	286.15	1.56	0.24	1.03
CoTiSb	15	199.08	126.29	312.74	1.58	0.24	1.01
	20	214.97	138.28	341.59	1.56	0.24	1.03
	25	233.26	152.15	374.93	1.47	0.23	1.04
	30	246.42	163.13	400.92	1.51	0.23	1.06

The bulk modulus to shear modulus (*B/G*) ratio defines a material plastic characteristic. According to the Pugh criterion (Greaves et al., 2019), the difference between ductile and brittle material is 1.75, which is the critical value. A high ratio of *B/G* indicates ductility, whereas a low number indicates the material's brittleness. In Table 4, the calculated results are displayed. As can be observed, all values of *B/G* are below the critical value of 1.75, demonstrating the brittle behavior of CoTiBi and CoTiSb alloys. The impact of pressure on the value of *B/G* is depicted in Figure 8. We observed that *B/G* decreased as pressure rises, suggesting that pressure can reduce the brittleness of these compounds. In addition, Poisson's ratio is also used to classify materials' bonding nature. The range of values lies between $0 < v < 0.5$. Values higher than 0.25 corresponds to materials associated with central forces and show better plasticity, whereas values lower than 0.25 correspond to materials dominated by covalent bonding (Zener & Siegel, 1949). Our current work shows that around the pressure values of 0, 5, 20, and 25 GPa, central forces are operational in CoTiBi, and at 10, 15, and 30 GPa, its dominated by covalent bonding. For CoTiSb, the values of *v* from 0 – 30 GPa indicate covalent bonding in this material. The degree of anisotropy in the solid structure is mostly determined by the isotropy factor (Khandy & Gupta, 2016). When $A = 1$, the compound is entirely isotropic. As shown in Table 4, both compounds have anisotropy factors that are $A > 1$, showing that they are elastically anisotropic. In Figure 8, the impact of pressure on the values of *A* is also reported. The value of *A* increases monotonically with pressure for CoTiBi, while, for CoTiSb it initially decreased and increased with a rise in pressure.

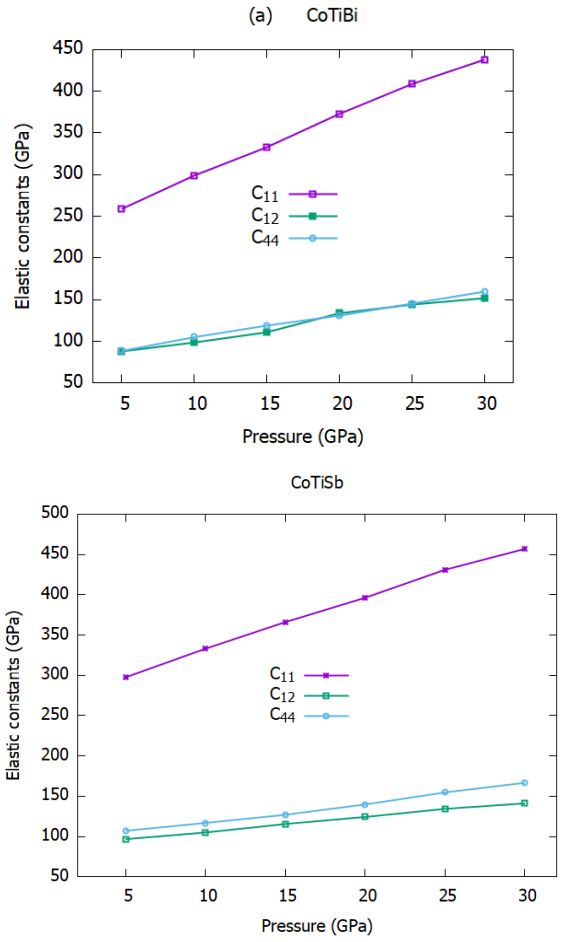

Figure 6: Variation of elastic constants (C_{11}, C_{12}, C_{44}) with pressure for (a) CoTiBi and (b) CoTiSb.

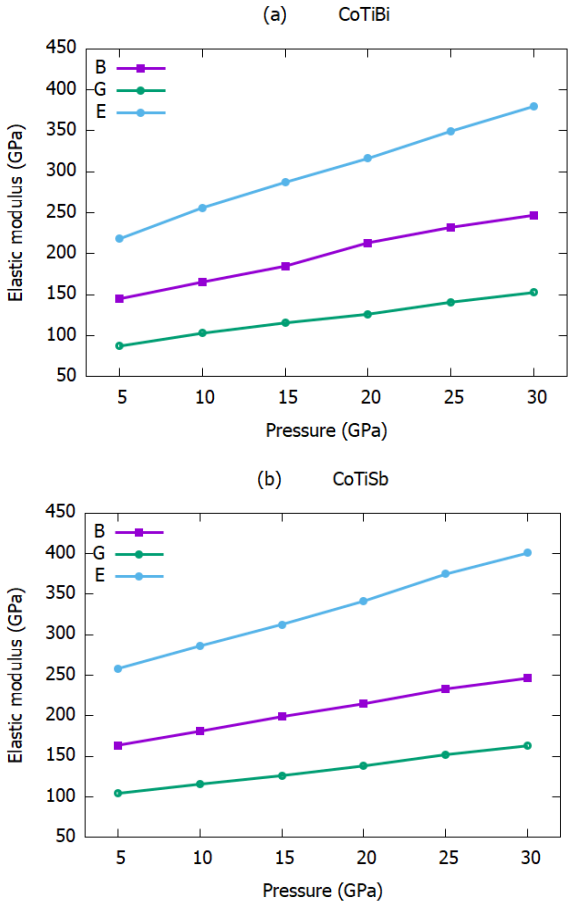

Figure 7: Variation of Young modulus (E), shear modulus (G), and bulk modulus (B) with pressure for (a) CoTiBi and (b) CoTiSb.

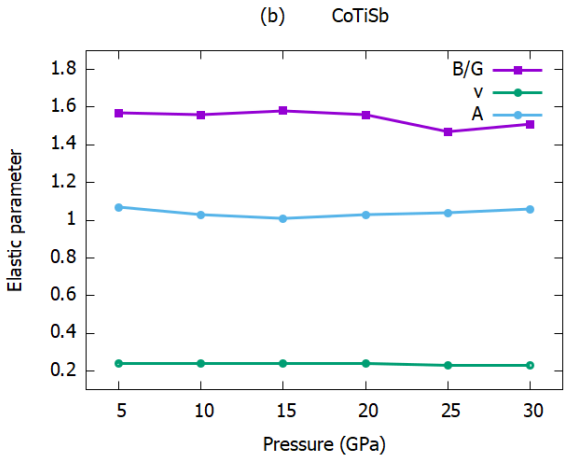

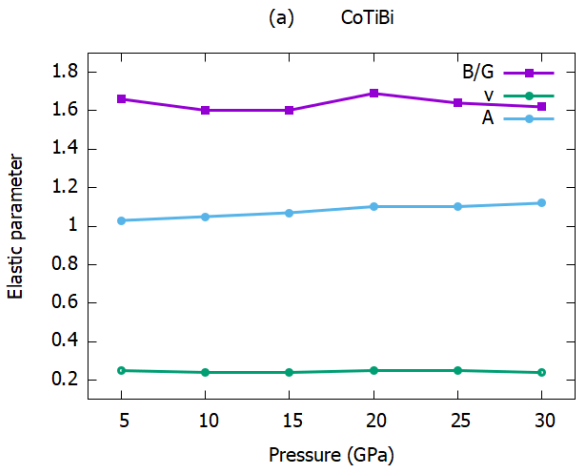

Figure 8: Variation of Pugh ratio, Poisson ratio (v), and isotropy factor (A) with pressure for (a) CoTiBi and (b) CoTiSb.

3.4 Thermodynamic properties

From the calculated elastic constants, we have determined the Debye temperature ($\boldsymbol{\Theta_D}$) and other related parameters at different pressures using the equations below (Khandy et al., 2018; Khandy & Gupta, 2016).

$$\Theta_D = \frac{h}{k_B}\left(\frac{3N}{4\pi V}\right)^{\frac{1}{3}} v_a \quad (12)$$

Where k_B, V, h, and N are the Boltzmann constant, volume, Planck's constant, number of atoms per formula unit. The mean sound velocity v_a calculated from the equations:

$$v_a = \sqrt[3]{3}\left(\frac{2}{v_t^3} + \frac{1}{v_l^3}\right)^{-\frac{1}{3}} \quad (13)$$

The transverse (v_t) and longitudinal (v_l) elastic sound velocites of CoToSb and CoTiBi are calculated from the bulk and shear modulus in Navier's equation (Schreiber et al., 1975).

$$v_l = \left(\frac{3B + 4G}{3\rho}\right)^{\frac{1}{2}} \quad (14)$$

$$v_t = \left(\frac{G}{\rho}\right)^{\frac{1}{2}} \quad (15)$$

The melting temperature and Gruneisen parameter calculated from Poisson ratio v are given as

$$T_m = (553\ (\mathrm{K}) + (5.911)\ \mathrm{C}_{11}) \pm 300\ \mathrm{K} \quad (16)$$

$$\gamma = \frac{3(1+v)}{2(2-2v)} \quad (17)$$

The Debye temperature is a very significant quantity in material science, which plays a crucial role in several properties of solid materials, such as thermal vibration of atoms, specific heat, melting point, and many other properties of solids (Boucetta, 2014; Qi et al., 2015). It also predicts the strength of bonds and the structural stability in solids. In order to gain a deeper insight into the lattice stability and thermodynamic properties under pressure, it is necessary to compute the values of $\boldsymbol{\Theta_D}$ under different pressure. Employing Eqs. (13) – (15), the results obtained are reported in Table 5. The pressure dependence of $\boldsymbol{\Theta_D}$ for both compounds is displayed in Figure 9. Values obtained reveal that the Debye temperature ($\boldsymbol{\Theta_D}$) increases with rising pressure for both

CoTiBi and CoTiSb. The values of $\boldsymbol{\Theta_D}$ at 5 and 30 GPa for CoTiSb are 377.02 and 488.27 K, respectively, and for CoTiSb are respectively 478.71 and 586.79 K. We observed that CoTiSb is more sensitive to pressure and has the highest $\boldsymbol{\Theta_D}$. Therefore, with rising pressure, the covalent bonds get stronger. CoTiSb possesses a stronger covalent bond and high thermal conductivity than CoTiBi semi-Heusler alloy. The melting temperature (T_m) was observed to increase monotonically with rising pressure for both CoTiSb and CoTiBi.

Table 5: Calculated pressure dependence of transverse sound velocity v_t (m/s), longitudinal sound velocity v_l (m/s), average sound velocity v_a (m/s) calculated from elastic moduli, Debye temperature Θ_D (K), and Gruneisen parameter (γ) under different pressure for CoTiBi and CoTiSb semi-Heuslers

Materials	Pressure	v_t(m/s)	v_l (m/s)	v_a (m/s)	Θ_D (K)	Γ	T_m (K) ±300
	5	2973.11	5144.44	3300.42	377.02	1.5	2,082.82
	10	3180.05	5451.05	3527.19	407.21	1.45	2,319.79
CoTiBi	15	3323.24	5690.04	3685.64	429.41	1.45	2,520.53
	20	3429.84	5964.13	3809.09	447.40	1.5	2,756.56
	25	3571.94	6179.87	3965.14	469.11	1.5	2,968.35
	30	3695.85	6348.65	4100.08	488.27	1.45	3,141.13
	5	3698.67	6300.71	4100.11	478.71	1.45	2,335.38
	10	3840.11	6537.01	4256.62	501.63	1.45	2,521.24
CoTiSb	15	3962.93	6759.91	4393.58	522.03	1.45	2,716.66
	20	4101.48	6970.08	4545.62	544.07	1.45	2,895.47
	25	4259.89	7212	4719.53	568.63	1.41	3,100.64
	30	4371.19	7371.53	4841.06	586.79	1.41	4,715.17

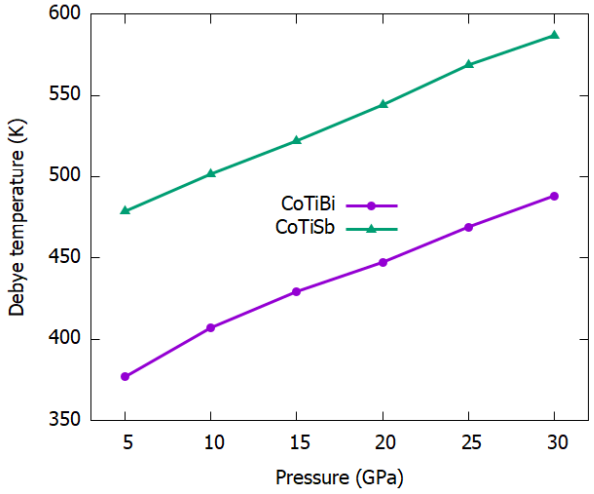

Figure 9: Variation of Debye temperature ($\boldsymbol{\Theta_D}$) with pressure for CoTiBi and CoTiSb.

Thermodynamic variables including Debye free energy (F), Debye entropy (S), Debye vibrational energy (E), and Debye heat capacity (C_v) have also been determined. Figure 10(a-d) displays the estimated C_v, S, F, and E in temperature range from 0 to 800 K. The specific heat of a solid can be used to describe how different thermodynamic

restrictions affect the behaviour of various materials. It also specifies how well the substance can hold heat. As a function of temperature, the phonon contribution dominates C_v. Figure 10(a) demonstrates that the Debye heat capacities C_v of CoTiSb and CoTiBi, obeys the Debye power law model, $C_v \propto T^3$ (Debye & Ann, 1912), as anticipated. This model accurately predicts heat capacity at low temperatures. At room temperature (298 K), it was found that the heat capacities of CoTiSb and CoTiBi respectively grew quickly to around 68.6 J/K/mol and 70.43 J/K/mol. And as the temperature increases, C_v converges to a constant value of 73.94 J/K/mol for CoTiSb and 74.22 J/K/mol for CoTiBi, indicating a strong agreement with the Dulong-Petit law (Petit and Dulong, 1981) at high temperatures. Since thermal agitation causes disorder, the entropy grows as the temperature rises. Figure 10(b) illustrates the entropy behavior with temperature. Figure 10(c) depicts the Debye free energy (F) of CoTiSb and CoTiBi, which decreases as temperature rises. The falling trend of F is extremely typical and gets worse as any natural process progresses. The entropy of any system determines the degree of F. Figure 10(d) illustrates a rising trend in the Debye vibrational energy (E) with temperature.

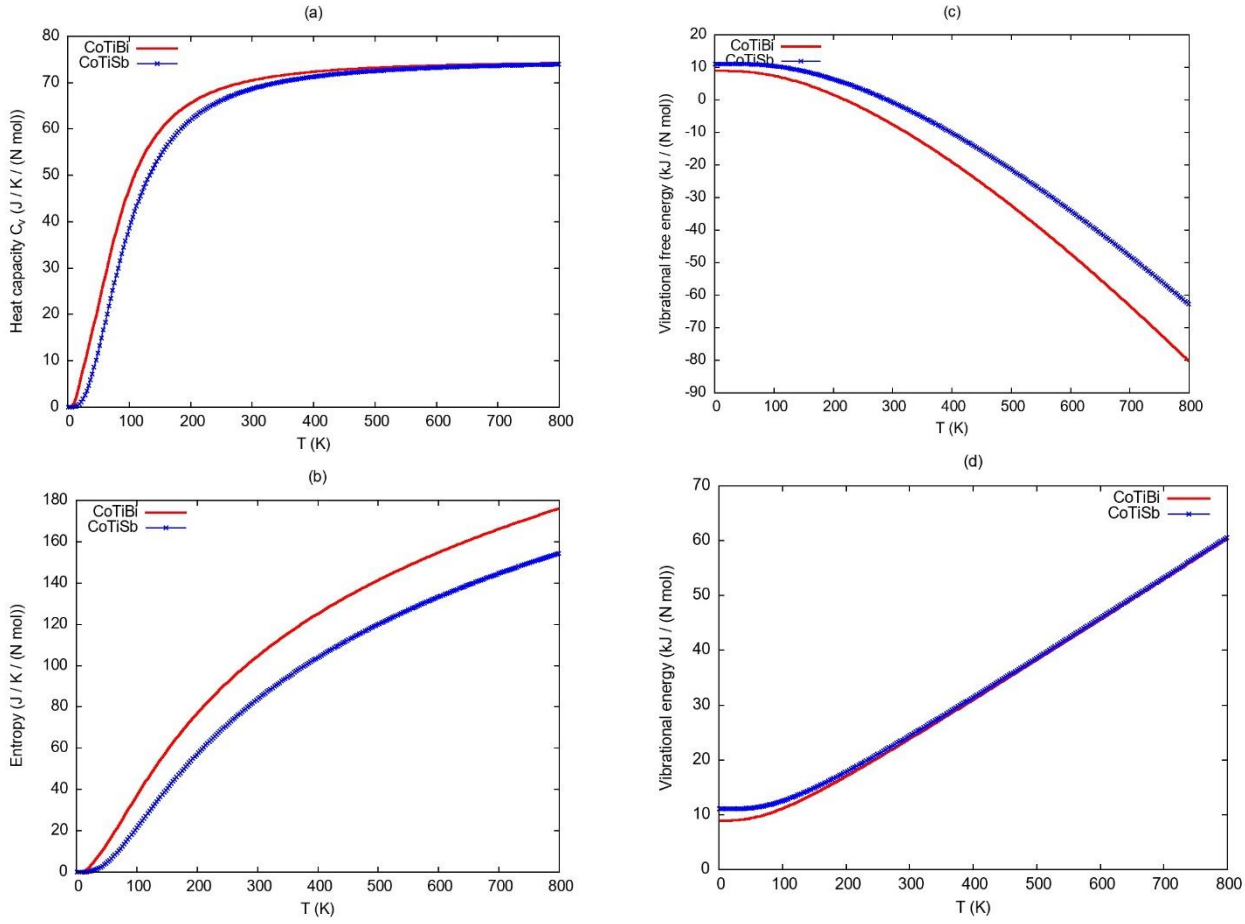

Figure 10: (a) Heat capacity (C_v), (b) entropy, (c) vibrational free energy, and (d) vibrational energy in the temperature range of (0 – 800) K.

4. CONCLUSION

The first principle computation using WIEN2K was suceefully emploed to optimize the structural properties, and study the phonon, electronic, thermodynamic,

and mechanical properties of CoTiSb and CoTiSb semi-Heusler alloys. The lattice constants of the semi-Heuslers were found to be 5.9 and 6.04 for CoTiSb and CoTiBi, respectively. Both alloys were found to be mechanically stable at zero and applied hydraustatic pressure by satisfying the well-established Born stability conditions. The Pugh ration of CoTiSb and CoTiBi was found to be less than 1.75, which indicates that these compounds are brittle in nature even at zero and applied hydraustatic pressure. The elastic constants and mechanical parameters were observed to be significantly influenced by presssure. The results obtained from the phonon dispersion curves confirmed that the alloys are thermodynamically stable. The heat capacity C_v was found to converge at 73.94 $JK^{-1}mol^{-1}$ and 74.22 $JK^{-1}mol^{-1}$ for CoTiSb and CoTiBi, reflecting the well-esblished Dulong-Petit law. From the elctronic properties, CoTiSb and CoTiBi were found to be an indirect band gap semiconductor with energy gap of 1.05 eV and 0.91 eV. The results obtained for elastic constants, lattice parameters, and energy gap for CoTiSb are in agreement with available data. However, there are no data to compare the results predicted for CoTiBi semi-Heusler. Therefore, the predicted results for CoTiBi may serve as reference to further studies.

REFERENCES

Ahmad Khandy, S., Kaur, K., Dhiman, S., Singh, J., and Kumar, V., (2021). Exploring thermoelectric properties and stability of half-Heusler PtXSn (X = Zr, Hf) semiconductors: A first principle investigation. *Computational Materials Science*, *188*. https://doi.org/10.1016/j.commatsci.2020.110232.

Ali, M. L., & Rahaman, M. Z. (2018). Investigation of different physical aspects such as structural, mechanical, optical properties and Debye temperature of Fe2ScM (M=P and As) semiconductors: A DFT-based first principles study. *International Journal of Modern Physics B*, *32*(10). https://doi.org/10.1142/S0217979218501217.

Benzoudji, F., Abid, O. M., Seddik, T., Yakoubi, A., Khenata, R., Meradji, H., Uğur, G., Uğur, S., & Ocak, H. Y. (2019). Insight into the structural, elastic, electronic, thermoelectric, thermodynamic and optical properties of MRhSb (M = Ti, Zr, Hf) half-Heuslers from ab initio calculations. *Chinese Journal of Physics*, *59*. https://doi.org/10.1016/j.cjph.2019.04.009.

Boucetta, S. (2014). Theoretical study of elastic, mechanical and thermodynamic properties of MgRh intermetallic compound. *Journal of Magnesium and Alloys*, *2*(1). https://doi.org/10.1016/j.jma.2014.04.001.

Casper, F., Graf, T., Chadov, S., Balke, B., & Felser, C. (2012). Half-Heusler compounds: Novel materials for energy and spintronic applications. In *Semiconductor Science and Technology* (Vol. 27, Issue 6). https://doi.org/10.1088/0268-1242/27/6/063001.

Chadov, S., Qi, X., Kübler, J., Fecher, G. H., Felser, C., & Zhang, S. C. (2010). Tunable multifunctional topological insulators in ternary Heusler compounds. *Nature Materials*, *9*(7). https://doi.org/10.1038/nmat2770.

Debye, P. , & Ann, D. (1912). Debye model. *Physik*, *39*, 789.

Dey, A., Sharma, R., Dar, S. A., & Raza, H. H. (2021). A Computational Investigation on Structural, Mechanical, Electronic, Magnetic, Thermoelectric, and Optical Properties of CrXPb (X = Sc, Ti) Half-Heusler Alloys. *Journal of Superconductivity and Novel Magnetism*, *34*(3). https://doi.org/10.1007/s10948-020-05791-w.

Dutt, R., Bhattacharya, J., & Chakrabarti, A.

(2022). Investigation of mechanical, lattice dynamical, electronic and thermoelectric properties of half Heusler chalcogenides: A DFT study. *Journal of Physics and Chemistry of Solids*, *167*. https://doi.org/10.1016/j.jpcs.2022.110704.

Enamullah, Enamullah, Sharma, S. K., & Ahmed, S. S. (2020). Transport properties of RuV-based half-Heusler semiconductors for thermoelectric applications: A computational study. *Journal of Physics Condensed Matter*, *32*(40). https://doi.org/10.1088/1361-648X/ab96f0.

Eperon, G. E., Paternò, G. M., Sutton, R. J., Zampetti, A., Haghighirad, A. A., Cacialli, F., & Snaith, H. J. (2015). Inorganic caesium lead iodide perovskite solar cells. *Journal of Materials Chemistry A*, *3*(39). https://doi.org/10.1039/c5ta06398a.

Fang, T., Zheng, S., Zhou, T., Yan, L., & Zhang, P. (2017). Computational prediction of high thermoelectric performance in p-type half-Heusler compounds with low band effective mass. *Physical Chemistry Chemical Physics*, *19*(6). https://doi.org/10.1039/c6cp07897d.

Fu, C., Bai, S., Liu, Y., Tang, Y., Chen, L., Zhao, X., & Zhu, T. (2015). *ARTICLE Realizing high figure of merit in heavy-band p-type half-Heusler thermoelectric materials*. https://doi.org/10.1038/ncomms9144.

Goldsmid, H. J., and Douglas, R. W. (1954). The use of semiconductors in thermoelectric refrigeration. *British Journal of Applied Physics*, *5*(12). https://doi.org/10.1088/0508-3443/5/12/513.

Greaves, G. N., Greer, A. L., Lakes, R. S., & Rouxel, T. (2019). Author Correction: Poisson's ratio and modern materials (Nature Materials, (2011), 10, 11, (823-837), 10.1038/nmat3134). In *Nature Materials* (Vol. 18, Issue 4). https://doi.org/10.1038/s41563-019-0319-2.

Guo, R., Wang, X., Kuang, Y., and Huang, B. (2015). First-principles study of anisotropic thermoelectric transport properties of IV-VI semiconductor compounds SnSe and SnS. *Physical Review B - Condensed Matter and Materials Physics*, *92*(11). https://doi.org/10.1103/PhysRevB.92.115202.

Hermet, P., Niedziolka, K., and Jund, P. (2013). A first-principles investigation of the thermodynamic and mechanical properties of Ni-Ti-Sn Heusler and half-Heusler materials. *RSC Advances*, *3*(44). https://doi.org/10.1039/c3ra43990a.

Hill, R. (1952). The elastic behaviour of a crystalline aggregate. *Proceedings of the Physical Society. Section A*, *65*(5). https://doi.org/10.1088/0370-1298/65/5/307.

Huang, S., Li, R. Z., Qi, S. T., Chen, B., & Shen, J. (2014). A theoretical study of the elastic and thermal properties of ScRu compound under pressure. *Physica Scripta*, *89*(6). https://doi.org/10.1088/0031-8949/89/6/065702.

Huang, Z. W., Zhao, Y. H., Hou, H., & Han, P. D. (2012). Electronic structural, elastic properties and thermodynamics of Mg 17Al 12, Mg 2Si and Al 2Y phases from first-principles calculations. *Physica B: Condensed Matter*, *407*(7). https://doi.org/10.1016/j.physb.2011.12.132.

Jaishi, D. R., Sharma, N., Karki, B., Belbase, B. P., Adhikari, R. P., & Ghimire, M. P. (2021). Electronic structure and thermoelectric properties of half-Heusler alloys NiTZ. *AIP Advances*, *11*(2). https://doi.org/10.1063/5.0031512.

Jamal, M., Jalali Asadabadi, S., Ahmad, I., & Rahnamaye Aliabad, H. A. (2014). Elastic constants of cubic crystals. *Computational Materials Science*, *95*. https://doi.org/10.1016/j.commatsci.2014.08.027.

Javed, M., Sattar, M. A., Benkraouda, M., & Amrane, N. (2020). Structural and mechanical stability, lattice dynamics and electronic structure of the novel CrVZ (Z = S, Se, & Te) half-Heusler alloys. *Materials Today Communications*, *25*.

https://doi.org/10.1016/j.mtcomm.2020.101519.

Jhi, S. H., Ihm, J., Loule, S. G., & Cohen, M. L. (1999). Electronic mechanism of hardness enhancement in transition-metal carbonitrides. *Nature*, *399*(6732). https://doi.org/10.1038/20148.

Jiao, Z. Y., Ma, S. H., Zhang, X. Z., & Huang, X. F. (2013). Pressure-induced effects on elastic and mechanical properties of TiC and TiN: A DFT study. *EPL*, *101*(4). https://doi.org/10.1209/0295-5075/101/46002.

Kaur, K., & Kumar, R. (2017). Ti based half Heusler compounds: A new on the screen with robustic thermoelectric performance. *Journal of Alloys and Compounds*, *727*, 1171–1177. https://doi.org/10.1016/J.JALLCOM.2017.08.216.

Khandy, S. A., and Gupta, D. C. (2016). Investigation of the transport, structural and mechanical properties of half-metallic REMnO3 (RE = Ce and Pr) ferromagnets. *RSC Advances*, *6*(100). https://doi.org/10.1039/c6ra19448f.

Khandy, S. A., Islam, I., Ganai, Z. S., Gupta, D. C., and Parrey, K. A. (2018). High-Temperature and High-Pressure Study of Electronic and Thermal Properties of PbTaO3 and SnAlO3 Metal Perovskites by Density Functional Theory Calculations. *Journal of Electronic Materials*, *47*(1). https://doi.org/10.1007/s11664-017-5785-1.

Kieven, D., Klenk, R., Naghavi, S., Felser, C., and Gruhn, T. (2010). I-II-V half-Heusler compounds for optoelectronics: Ab initio calculations. *Physical Review B - Condensed Matter and Materials Physics*, *81*(7). https://doi.org/10.1103/PhysRevB.81.075208.

Korozlu, N., Colakoglu, K., Deligoz, E., and Aydin, S. (2013). The elastic and mechanical properties of MB12 (M = Zr, Hf, Y, Lu) as a function of pressure. *Journal of Alloys and Compounds*, *546*. https://doi.org/10.1016/j.jallcom.2012.08.062.

Kumarasinghe, C., and Neophytou, N. (2019). Band alignment and scattering considerations for enhancing the thermoelectric power factor of complex materials: The case of Co-based half-Heusler alloys. *Physical Review B*, *99*(19). https://doi.org/10.1103/PhysRevB.99.195202.

Lee, E. K., Yin, L., Lee, Y., Lee, J. W., Lee, S. J., Lee, J., Cha, S. N., Whang, D., Hwang, G. S., Hippalgaonkar, K., Majumdar, A., Yu, C., Choi, B. L., Kim, J. M., & Kim, K. (2012). Large thermoelectric figure-of-merits from SiGe nanowires by simultaneously measuring electrical and thermal transport properties. *Nano Letters*, *12*(6). https://doi.org/10.1021/nl300587u.

Ma, J., Hegde, V. I., Munira, K., Xie, Y., Keshavarz, S., Mildebrath, D. T., Wolverton, C., Ghosh, A. W., & Butler, W. H. (2017). Computational investigation of half-Heusler compounds for spintronics applications. *Physical Review B*, *95*(2). https://doi.org/10.1103/PhysRevB.95.024411.

Malica, C., & Dal Corso, A. (2021). Quasi-harmonic thermoelasticity of palladium, platinum, copper, and gold from first principles. *Journal of Physics Condensed Matter*, *33*(47). https://doi.org/10.1088/1361-648X/ac2041.

Mehl, M. J. (1993). Pressure dependence of the elastic moduli in aluminum-rich Al-Li compounds. *Physical Review B*, *47*(5). https://doi.org/10.1103/PhysRevB.47.2493

Murnaghan, F. D. (1944). The Compressibility of Media under Extreme Pressures. *Proceedings of the National Academy of Sciences*, *30*(9). https://doi.org/10.1073/pnas.30.9.244.

Nenuwe, O. N., & Judith, U. (2021). Elastic and mechanical properties of cubic metal arsenides (Ga, In and Al) under high-pressure:

a simulation study. *Ruhuna Journal of Science*, *12*(1). https://doi.org/10.4038/rjs.v12i1.96.

Nenuwe, N., & Agbalagba, E. O. (2021). High-pressure Effect of Elastic and Mechanical Properties of Hexagonal Gallium Nitride. *VNU Journal of Science: Mathematics - Physics*, *37*(2). https://doi.org/10.25073/2588-1124/vnumap.4555.

Osafile, O. E., & Nenuwe, O. N. (2021). Lattice dynamics and thermodynamic responses of XNbSn half-heusler semiconductors: A first-principles approach. *Journal of the Nigerian Society of Physical Sciences*, *3*(2). https://doi.org/10.46481/jnsps.2021.174.

Ouardi, S., Fecher, G. H., Felser, C., Schwall, M., Naghavi, S. S., Gloskovskii, A., Balke, B., Hamrle, J., Postava, K., Piatora, J., Ueda, S., & Kobayashi, K. (2012). Electronic structure and optical, mechanical, and transport properties of the pure, electron-doped, and hole-doped Heusler compound CoTiSb. *Physical Review B - Condensed Matter and Materials Physics*, *86*(4). https://doi.org/10.1103/PhysRevB.86.045116.

Parvin, F., Hossain, M. A., Ahmed, I., Akter, K., & Islam, A. K. M. A. (2021). First-principles calculations to investigate mechanical, optoelectronic and thermoelectric properties of half-Heusler p-type semiconductor BaAgP. *Results in Physics*, *23*. https://doi.org/10.1016/j.rinp.2021.104068.

Perdew, J. P., Burke, K., & Ernzerhof, M. (1997). Erratum: Generalized gradient approximation made simple (Physical Review Letters (1996) 77 (3865)). In *Physical Review Letters* (Vol. 78, Issue 8). https://doi.org/10.1103/PhysRevLett.78.1396.

Petit, A. T., & Dulong P. L. (1981). *Research on some important points of the theory of heat*. *10*, 395.

Poudel, B., Hao, Q., Ma, Y., Lan, Y., Minnich, A., Yu, B., Yan, X., Wang, D., Muto, A., Vashaee, D., Chen, X., Liu, J., Dresselhaus, M. S., Chen, G., & Ren, Z. (2008). High-thermoelectric performance of nanostructured bismuth antimony telluride bulk alloys. *Science*, *320*(5876). https://doi.org/10.1126/science.1156446.

Poudeu, P. F. P., D'Angelo, J., Kong, H., Downey, A., Short, J. L., Pcionek, R., Hogan, T. P., Uher, C., & Kanatzidis, M. G. (2006). Nanostructures versus solid solutions: Low lattice thermal conductivity and enhanced thermoelectric figure of merit in Pb9.6Sb 0.2Te10-xSex bulk materials. *Journal of the American Chemical Society*, *128*(44). https://doi.org/10.1021/ja0647811.

Pugh, S. F. (1954). XCII. Relations between the elastic moduli and the plastic properties of polycrystalline pure metals. *The London, Edinburgh, and Dublin Philosophical Magazine and Journal of Science*, *45*(367). https://doi.org/10.1080/14786440808520496.

Qi, L., Jin, Y., Zhao, Y., Yang, X., Zhao, H., & Han, P. (2015). The structural, elastic, electronic properties and Debye temperature of Ni3Mo under pressure from first-principles. *Journal of Alloys and Compounds*, *621*. https://doi.org/10.1016/j.jallcom.2014.10.015.

Ramasamy, P., Lim, D. H., Kim, B., Lee, S. H., Lee, M. S., & Lee, J. S. (2016). All-inorganic cesium lead halide perovskite nanocrystals for photodetector applications. *Chemical Communications*, *52*(10). https://doi.org/10.1039/c5cc08643d.

Rogl, G., Grytsiv, A., Gürth, M., Tavassoli, A., Ebner, C., Wünschek, A., Puchegger, S., Soprunyuk, V., Schranz, W., Bauer, E., Müller, H., Zehetbauer, M., & Rogl, P. (2016). Mechanical properties of half-Heusler alloys. *Acta Materialia*, *107*. https://doi.org/10.1016/j.actamat.2016.01.031.

Sailuam, W., Fongkaew, I., Limpijumnong, S., & Phacheerak, K. (2022). A first principles investigation on the structural, elastic, and mechanical properties of MAX phase M3AlC2 (M= Ta, Ti, V) as a function of pressure. *Computational Condensed Matter*, *30*. https://doi.org/10.1016/j.cocom.2021.e00638.

Sarwan, M., Shukoor V, A., Shareef M, F., & Singh, S. (2021). A first principle study of structural, elastic, electronic and thermodynamic properties of Half-Heusler compounds; YNiPn (Pn=As, sb, and bi). *Solid State Sciences*, *112*. https://doi.org/10.1016/j.solidstatesciences.2020.106507.

Schreiber, E., Anderson, O. L., Soga, N., & Bell, J. F. (1975). Elastic Constants and Their Measurement. *Journal of Applied Mechanics*, *42*(3). https://doi.org/10.1115/1.3423687.

Schwarz, K., & Blaha, P. (2003). Solid state calculations using WIEN2k. *Computational Materials Science*, *28*(2). https://doi.org/10.1016/S0927-0256(03)00112-5.

Schwarz, K., Blaha, P., & Madsen, G. K. H. (2002). Electronic structure calculations of solids using the WIEN2k package for material sciences. *Computer Physics Communications*, *147*(1–2). https://doi.org/10.1016/S0010-4655(02)00206-0.

Shi, F., Si, M. S., Xie, J., Mi, K., Xiao, C., & Luo, Q. (2017). Hybrid density functional study of bandgaps for 27 new proposed half-Heusler semiconductors. *Journal of Applied Physics*, *122*(21). https://doi.org/10.1063/1.4998145.

Sjöstedt, E., Nordström, L., & Singh, D. J. (2000). Alternative way of linearizing the augmented plane-wave method. *Solid State Communications*, *114*(1), 15–20. https://doi.org/10.1016/S0038-1098(99)00577-3.

Toboła, J., Pierre, J., Kaprzyk, S., Skolozdra, R. v., & Kouacou, M. A. (1998). Crossover from semiconductor to magnetic metal in semi-Heusler phases as a function of valence electron concentration. *Journal of Physics Condensed Matter*, *10*(5). https://doi.org/10.1088/0953-8984/10/5/011.

Tyuterev, V. G., & Vast, N. (2006). Murnaghan's equation of state for the electronic ground state energy. *Computational Materials Science*, *38*(2). https://doi.org/10.1016/j.commatsci.2005.08.012.

Wang, J., Yip, S., Phillpot, S. R., & Wolf, D. (1993). Crystal instabilities at finite strain. *Physical Review Letters*, *71*(25). https://doi.org/10.1103/PhysRevLett.71.4182

Wani, T. A., Prasad, T., Ma'Aruf, A., Shitu, A., & Ahuja, R. S. (2021). Elastic and mechanical properties of titanium diboride under high pressure. *Materials Today: Proceedings*, *49*. https://doi.org/10.1016/j.matpr.2021.09.349.

Wei, J., & Wang, G. (2018). Thermoelectric and optical properties of half-Heusler compound TaCoSn: A first-principal study. *Journal of Alloys and Compounds*, *757*. https://doi.org/10.1016/j.jallcom.2018.05.037.

Yakoubi, A., Baraka, O., & Bouhafs, B. (2012). Structural and electronic properties of the Laves phase based on rare earth type BaM 2 (M=Rh, Pd, Pt). *Results in Physics*, *2*. https://doi.org/10.1016/j.rinp.2012.06.001.

Zener, C. M., & Siegel, S. (1949). Elasticity and Anelasticity of Metals. *The Journal of Physical and Colloid Chemistry*, *53*(9). https://doi.org/10.1021/j150474a017.

Zhu, H., He, R., Mao, J., Zhu, Q., Li, C., Sun, J., Ren, W., Wang, Y., Liu, Z., Tang, Z., Sotnikov, A., Wang, Z., Broido, D., Singh, D. J., Chen, G., Nielsch, K., & Ren, Z. (2018). Discovery of ZrCoBi based half Heuslers with high

thermoelectric conversion efficiency. *Nature Communications*, *9*(1). https://doi.org/10.1038/s41467-018-04958-3.

Zhu, H., Mao, J., Li, Y., Sun, J., Wang, Y., Zhu, Q., Li, G., Song, Q., Zhou, J., Fu, Y., He, R., Tong, T., Liu, Z., Ren, W., You, L., Wang, Z., Luo, J., Sotnikov, A., Bao, J., … Ren, Z. (2019). Discovery of TaFeSb-based half-Heuslers with high thermoelectric performance. *Nature Communications*, *10*(1). https://doi.org/10.1038/s41467-018-08223-5.